

# Structure-dilute solution property relationships of comb-like macromolecules in a good solvent

Robert J. S. Ivancic, Sara V. Orski, and Debra J. Audus\*

*Materials Science and Engineering Division, National Institute of Standards and Technology, Gaithersburg, Maryland 20899, United States*

E-mail: [debra.audus@nist.gov](mailto:debra.audus@nist.gov)

Phone: (301) 975-4364

## Abstract

The structural characterization of branched polymers still poses experimental challenges despite their technological potential. This lack of clarity is egregious in linear low-density polyethylene (LLDPE), a common industrial plastic. Here, we design a coarse-grain, implicit solvent molecular dynamics model for LLDPE in 1,2,4-trichlorobenzene, a canonical good solvent, that replicates all-atom simulations and experiments. We employ this model to test the relationship between the contraction factors, the ratios of branched to linear dilute solution properties. In particular, we relate the contraction factor of the radius of gyration to that of the intrinsic viscosity and the hydrodynamic radius. The contraction exponents are constant as we vary branch length and spacing in contrast to theoretical expectations. We use this observation to develop a general theory for the dilute solution properties of linear polymers with linear side-chain branches, comb-like macromolecules, in a good solvent and validate the theory by generating master curves for LLDPE.

# Introduction

Research dating to the 1960s establishes the foundation for the theory of linear polymers in good solvents.<sup>1</sup> However, understanding the next simplest architecture, linear polymers with linear side-chain branches, remains a challenge. Branches increase the mass per backbone length of the polymer chain. While prior work demonstrates this effect typically leads to a decrease in the dilute solution properties at a given molar mass,<sup>2-4</sup> these expectations do not constitute a complete theory. This lack of understanding makes it difficult to characterize structure-property relationships for comb-like macromolecules that have applications in numerous, novel technologies, such as photonic crystals,<sup>5</sup> chemotherapy,<sup>6</sup> and drug delivery.<sup>7</sup> These applications do not consider less novel but industrially important comb-like polymers such as linear low-density polyethylene (LLDPE), which combined with low-density polyethylene (LDPE) comprises 16% of the plastics market worldwide.<sup>8</sup> The popularity of LLDPE in applications from food packaging to playgrounds stems from its flexibility compared to high-density polyethylene (HDPE) and its improved stress-crack resistance, puncture resistance, and optical clarity compared to LDPE.<sup>9,10</sup> These properties and the properties of comb-like polymers generally depend on the the polymer's precise macromolecular architecture. An improved understanding of the relationship between comb-like polymers' dilute solution properties and architecture would provide a useful tool to infer this architecture from measurable quantities. Such a theory would enable the simultaneous tuning of multiple properties or the extrapolation of properties from previously studied structure-property relationships.

Studies of polymer dilute solution properties typically consider the scaling relationships of the radius of gyration ( $R_g$ ), intrinsic viscosity ( $[\eta]$ ), and hydrodynamic radius ( $R_h$ ) for a given architecture

$$R_g = K_{R_g} M^{\nu_{R_g}} \tag{1}$$

$$[\eta] = K_{[\eta]} M^{\nu_{[\eta]}} \tag{2}$$

$$R_h = K_{R_h} M^{\nu_{R_h}} \quad (3)$$

where  $M$  is the molar mass. Here, the radius of gyration is the root-mean-square distance from the center of mass and represents a *structural* measure of polymer size. The other two properties represent *dynamic* measures of polymer stiffness and size. In particular, intrinsic viscosity measures the increase in viscosity due to an infinitesimal amount of polymer solute. In contrast, the hydrodynamic radius measures the radius of a hard sphere that diffuses at the same rate as the polymer solute.

The scaling exponents ( $\nu_i$ ) and prefactors ( $K_i$ ) of Eqs. 1-3 depend on solvent quality and architecture. For example, a linear polymer behaves as an ideal chain in a theta solvent, and the scaling exponents tend to  $\nu_i = 1/2$ .<sup>11</sup> In a good solvent, these exponents increase due to excluded volume interactions. The simple Flory theory suggests  $\nu_{R_g} = 3/5$ ,<sup>1</sup> whereas the more precise Borel resummation indicates  $\nu_{R_g} = 0.588 \pm 0.001$ .<sup>12</sup> The precise values of  $\nu_{[\eta]}$  and  $\nu_{R_h}$  depend on the nature of the polymer-solvent interactions. In the non-draining limit, solvent molecules inside the polymer coil move with it.<sup>11</sup> This assumption implies  $R_h \sim R_g \implies \nu_{R_h} = \nu_{R_g}$  and leads to the Flory-Fox relationship that indicates  $[\eta] \sim R_g^3/M \implies \nu_{[\eta]} = 3\nu_{R_g} - 1$ .<sup>11</sup> Experimentally, these relationships are reasonable estimates but imperfect due to drainage effects.<sup>13,14</sup> Typically, experiments find  $0.70 \leq \nu_{[\eta]} \leq 0.80$  in good solvents in contrast to the predicted  $\nu_{[\eta]} = 0.764$  found using the above theory with the Borel resummation exponent.<sup>11</sup> The prefactors of Eqs. 1-3 are more difficult to quantify. While we can compute the prefactor of a linear polymer's radius of gyration in a theta solvent using rotational isomeric state theory,<sup>1</sup> this approach cannot compute the prefactors for dynamic quantities such as  $[\eta]$  and  $R_h$ . The computation of these values from structural information is still an area of active research.<sup>15,16</sup>

The above arguments do not account for changes in these scaling relationships caused by the presence of branches. A quantitative method to explore these changes is through contraction factors ( $g_i$ ), the ratio of branched to linear dilute solution properties. Specifically,

we consider

$$g_{R_g^2} = \left\langle \frac{(R_{g,b})^2}{(R_{g,l})^2} \right\rangle \quad (4)$$

$$g_{[\eta]} = \left\langle \frac{[\eta]_b}{[\eta]_l} \right\rangle \quad (5)$$

$$g_{R_h} = \left\langle \frac{R_{h,b}}{R_{h,l}} \right\rangle \quad (6)$$

where the subscripts  $l$  and  $b$  denote whether we measure a dilute solution property for linear or branched polymers. If the linear and branched dilute solution properties follow the different scaling exponents, we must specify some mass range over which to perform these averages denoted by the angle brackets in Eqs. 4-6. Otherwise, the contraction factor simplifies to a ratio of  $K_{i,b}$  to  $K_{i,l}$ . We take the contraction of  $R_h$  rather than  $R_h^2$  because the linear version is what is measured experimentally and has been considered in the literature previously.<sup>17</sup> Furthermore, these quantities are typically less than unity due to increased mass per backbone length from branching.

Because measuring the radius of gyration through light scattering is imprecise compared to measuring intrinsic viscosity, theorists have invested a significant amount of research into relating the contraction factor of the radius of gyration to that of intrinsic viscosity. The Flory-Fox relationship gives  $g_{[\eta]} = g_{R_g^2}^{3/2}$  for non-draining linear polymers, whereas Zimm and Kilb<sup>18</sup> indicate  $g_{[\eta]} = g_{R_g^2}^{1/2}$  for non-draining star polymers. These distinct contraction exponents (3/2 and 1/2) indicate at least two scaling regimes of polymer dilution solution properties in good solvent.

This observation leads to the question: How does one relate the radius of gyration and intrinsic viscosity contraction factors in the case of comb-like macromolecules? One may expect that they behave as linear polymers. Conversely, Berry<sup>19</sup> suggests the contraction exponent may smoothly vary as macromolecular architecture is changed between the extremes of star and linear polymers. Although not well studied, we can hypothesize a similar relationship between the contraction factors of the hydrodynamic radius and the radius of

gyration. Thus, we may anticipate

$$g_{[\eta]} = g_{R_g^2}^{\epsilon_{[\eta]}} \tag{7}$$

$$g_{R_h} = g_{R_g^2}^{\epsilon_{R_h}} \tag{8}$$

where  $\epsilon_{[\eta]}$  and  $\epsilon_{R_h}$  are the contraction exponents. In the case of comb-like macromolecules behaving like linear polymers, we expect  $\epsilon_{[\eta]} = 3/2$  from the Flory-Fox relationship and  $\epsilon_{R_h} = 1/2$  from the non-draining model. If Berry’s suggestion holds,<sup>19</sup> we should expect these contraction exponents to vary with branch length and spacing.

Experimentally, significant uncertainty exists in the measurement of these contraction exponents. Accurate experiments must use size exclusion chromatography combined with triple detection to reduce uncertainty due to postfractionation, as well as a synthetic chemistry that allows for homogeneous architectures due to the inability of size exclusion chromatography to resolve architectural heterogeneity.<sup>3</sup> Initially, star polymers were found to have  $\epsilon_{[\eta]} = 0.6$  for 12 arms in both good and theta solvents,<sup>20</sup> but later it was shown that this contraction exponent increased to  $\epsilon_{[\eta]} \approx 1$  as the number of arms was increased from 3 to 128.<sup>21</sup> In a good solvent, comb-like polystyrene has  $0.9 \leq \epsilon_{[\eta]} \leq 1.2$ ,<sup>3,22,23</sup> while comb-like polyethylene has  $0.92 \leq \epsilon_{[\eta]} \leq 1.5$ <sup>2,24,25</sup> in good solvent. To complicate matters further, these contraction exponents change as a function of solvent quality.<sup>3</sup>

The lack of high quality experimental data to test theories and benchmark noisy industrial feedstocks is particularly egregious for a plastic as common and useful as LLDPE. Because generating precise experimental data is challenging, one may attempt to turn to molecular dynamics simulations to provide high-quality measurements of LLDPE in a good solvent, but existing models are inadequate. While chemically specific polyethylene coarse-grain models have been designed,<sup>26-29</sup> these models focus on the melt rather good solvent properties of polyethylene and do not include branching. Panizon *et al.*<sup>30</sup> develop a model of LLDPE with branches of 4 carbons that is compatible with the MARTINI<sup>31</sup> potential, but it requires the use of an explicit solvent that limits its use to small molecules. Another method

by Zhang and coworkers<sup>32</sup> utilizes an implicit solvent coarse-grain, bead-spring model to explore the effect of nonbonded interactions on solvent quality. They subsequently compare their results to experiments of LLDPE with precise branch lengths and spacings and find qualitative agreement for a variety of dilute solution properties. However, this model does not include chemically specific local interactions such as bond angles that prohibit quantitative agreement. More recently, López-Barrón *et al.*<sup>25</sup> simulate bottlebrush polymers in good solvent using an implicit solvent, united atom model. This model uses united-atom bonds<sup>33</sup> and modifies six nonbonded parameters to match all-atom  $R_g$  data. However, the atomic resolution of this model inherently limits the range of molar mass that can be simulated in a timely manner even with advanced sampling techniques.

To remedy these issues, we build a coarse-grain, implicit solvent model of LLDPE in 1,2,4-trichlorobenzene, a standard polymer-good solvent pair.<sup>2,4,34</sup> We design this coarse-grain potential to reproduce all-atom bond distributions of monomers on short-length scales and experimental results on long-length scales using the precisely synthesized LLDPE by Orski and coworkers<sup>4</sup> both for inspiration and benchmarking. This coarse-grain potential allows us to efficiently extend the library of good solvent dilute solution structure-property relationships of LLDPE with precise branch lengths ( $L$  carbons) and branch spacings ( $S$  carbons), *i.e.*, the number of carbons between branch points, to significantly larger branch spacings. This regime is well beyond what is currently experimentally accessible through precise synthesis techniques such as ring-opening metathesis polymerization.<sup>35</sup> Additionally, these results provide a measure of the hydrodynamic radius which was not measured in the original experiments. Our data allows us to explicitly test theoretical and experimental predictions for  $\epsilon_{[\eta]}$  and confirm the hypothesized relationship in Eq. 8 for  $\epsilon_{R_h}$ . We find our scaling and contraction exponents are *constant* with respect to branch length and spacing but also do not match theoretical expectations ( $\epsilon_{[\eta]} = 1.13 \pm 0.03 \neq 3/2$  and  $\epsilon_{R_h} = 0.33 \pm 0.02 \neq 1/2$ ). Noting our scaling and contraction exponents are constant suggests comb-like polymers form a scaling regime, *i.e.*, a set of polymer architectures in which all parameters that

define the architecture share the same scaling form. We build upon these observations to generate a generic model to predict dilution solution properties of comb-like macromolecules in good solvent. This model collapses our coarse-grain LLDPE data at all branch lengths and spacings onto a single master curve for each dilute solution property. We then discuss future applications of our coarse-grain model and the ramifications of our theory, especially on approach to the bottlebrush limit (large  $L$  and small  $S$ ).

## Methods

To generate our coarse-grain implicit solvent model, we simulate two small polyolefin molecules in 1,2,4-trichlorobenzene at  $T = 135$  °C and  $P = 101$  kPa (1 atm) using the all-atom optimized potential for liquids simulation force field (OPLS-AA).<sup>36</sup> This force field has been optimized to obtain accurate descriptions of liquid state properties<sup>37</sup> and has been used to build coarse-grain polyethylene models in the past.<sup>28,29</sup> In order to simulate the dilute regime, we carry out these simulations with 264 solvent molecules and a single polyolefin oligomer. We choose the amount of solvent such that the polymer avoids self-interactions. A more detailed description of these simulations and the small molecules used is provided in the Supporting Information, Fig. S1.

Our coarse-grain scheme in Fig. 1A contains three types of monomers: main chain monomers ( $A$ ), branch monomers ( $B$ ), and connector monomers. Main chain monomers are ethylene units containing 4 carbons. Branch monomers are the same as main chain monomers, but they contain an extra carbon bond on the third carbon atom to allow branching. Connector monomers attach to branch monomers using these extra carbon bonds. These monomers either contain 4 carbons ( $C_4$ ) or 2 carbons ( $C_2$ ), as shown in red on the left and right of Fig. 1A. Designing our model with two types of connector monomers allows for additional precision in the branch lengths of LLDPE that we can build. We convert the all-atom bond length, angle, and dihedral monomer distributions to coarse-grain potentials

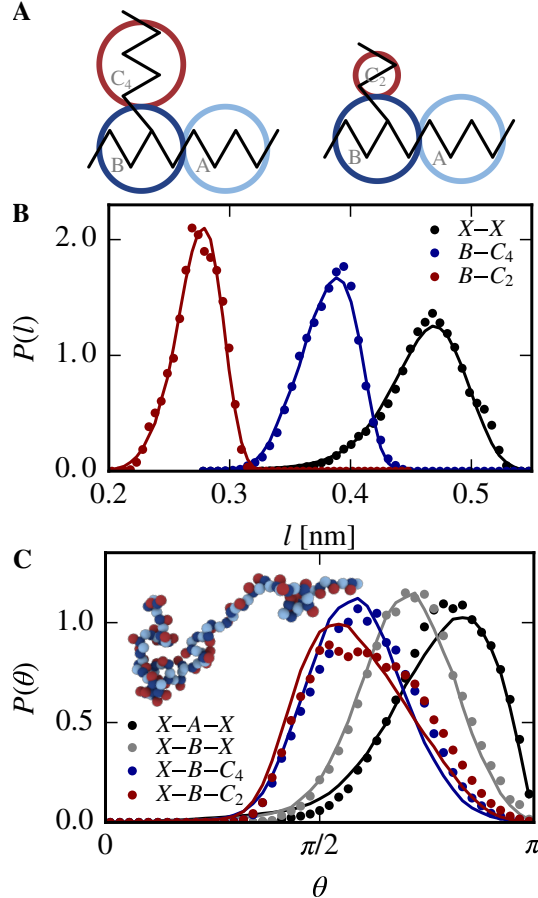


Figure 1: **Comparison of all-atom and coarse-grain bond distributions.** (A) The image shows a schematic of our coarse-grain model. Lines represent polyolefin in bond line notation, while light and dark blue circles represent main-chain (A) and branch (B) monomers. Red circles denote the 4-carbon ( $C_4$ , left) or 2-carbon ( $C_2$ , right) connector monomers. (B) The plot presents example distributions of bond lengths for bonds  $X-X$ ,  $B-C_4$ , and  $B-C_2$  in black, blue, and red, where  $X$  indicates either a  $B$  or  $A$  monomer. Dots and lines represent all-atom and coarse-grain monomer distributions. (C) The plot shows selected distributions of bond angles  $X-A-X$ ,  $X-B-X$ ,  $X-B-C_4$ , and  $X-B-C_2$  in black, grey, blue, and red. The inset shows a snapshot of a coarse-grain LLDPE with a branch spacing of  $S = 8$  carbons, a branch length of  $L = 4$  carbons, and molar mass of  $M = 8.3 \times 10^3$  g/mol. The colors correspond to the coarse-grain scheme in (A).

using the first step of Boltzmann inversion.<sup>29</sup>

To obtain our nonbonded interactions, we first fit a 12-6 Lennard-Jones interaction,  $U_{\text{LJ}}^n(r) = 4\epsilon((\frac{\sigma_n}{r})^{12} - (\frac{\sigma_n}{r})^6)$  for  $r < r_c = 15$  nm, to the  $n = 2$  and 4-carbon coarse-grain nonbonded tabular potentials for polyethylene melts found in Salerno and coworkers.<sup>29</sup> This procedure gives a similar result to the MARTINI nonbonded potential for the 4-carbon

case.<sup>30</sup> We display the fits to this data in the Supporting Information, Fig. S5. We then set our implicit solvent, nonbonded interaction to be

$$U^n(r) = \alpha U_{LJ}^n(r) + (1 - \alpha) U_{WCA}^n(r) \quad (9)$$

where  $U_{WCA}^n(r)$  is a Weeks-Chandler-Andersen (WCA) interaction<sup>38</sup> and  $\alpha$  is a parameter that modulates the solvent quality. A WCA interaction is the purely repulsive part of the Lennard-Jones interaction. The advantage of this form is that it allows us to transform the potential from a purely repulsive potential ( $\alpha = 0$ ) to the melt potential ( $\alpha = 1$ ) without changing the short-range, repulsive nonbonded forces. We expect such behavior because there is no solvent between the monomers to mediate their interactions at distances within the range of the WCA potential. We use standard Lorentz-Berthelot<sup>39</sup> combination rules to parameterize the cross-interaction between the  $n = 2$  and 4 carbon beads. Finally, we choose  $\alpha = 0.2$  to ensure scaling exponents that are consistent with experimental values for polyethylene.<sup>2,4</sup> Additional details are provided in the Supporting Information, Fig. S6. Changes in  $\alpha$  do not affect the coarse-grain distributions of Figs. 1A and 1B for  $\alpha \in [0, 1]$ . We list the parameters for all bonded and nonbonded interactions in the Supporting Information, Tables S1, S2, S3, and S4.

We perform our coarse-grain polymer simulations using the Large-scale Atomic/Molecular Massively Parallel Simulator (LAMMPS)<sup>40</sup> utilizing a Langevin thermostat and timestep of 8 fs when using  $C_2$  monomers or 10 fs otherwise. All dilute solution properties are estimated using ZENO. For every snapshot, ZENO models the polymer as a collection of hard spheres, taken to have a radius of 2.8 nm for monomers with 4 carbons and 2.1 nm for monomers with 2 carbons, and computes the various dilute solution properties. The radius of gyration squared is computed directly while the hydrodynamic radius and intrinsic viscosity are calculated by invoking an electrostatic-hydrodynamic analogy.<sup>41,42</sup> Specifically, the hydrodynamic radius is taken to be equal to the capacitance, while the intrinsic viscosity is taken to

be proportional to the intrinsic conductivity, with a prefactor that varies slowly with shape as detailed in Ref. 42. We choose the radii of the hard spheres to correspond to minimum radii to maintain chain connectivity throughout our simulations. The properties are then averaged over all the snapshots. ZENO has previously been shown to capture the experimental dilute solution properties.<sup>14,25,43,44</sup> We find that for this solvent-solute combination, ZENO overestimates the experimentally measured intrinsic viscosity by approximately 30%. Similar overestimation of intrinsic viscosity seems to occur in all molecular dynamics studies attempting to model this solvent-solute pair with ZENO.<sup>25,32</sup> This deviation could be due to an inaccurate empirical prefactor for this class of shapes; however, we leave the exploration of why this deviation occurs to future work but find that multiplying all our intrinsic viscosity data by a best-fit constant  $c = 0.68$  aligns our simulations with experiments. To speed up the mixing rate of these simulations, we use parallel tempering<sup>45</sup> and perform averaging using the multistate Bennett acceptance ratio estimator.<sup>46</sup> To guarantee proper mixing, we monitor the radius of gyration as a function of simulation time and ensure it decorrelates multiple times for a given simulation. We discard the first decorrelation time from our analysis so that our initial configurations are properly equilibrated.

## Results

### Coarse-grain model

We compare the all-atom to coarse-grain monomer distributions for selected bond lengths and angles in Figs. 1B and 1C, respectively. Other distributions are available in the Supporting Information, Figs. S2, S3, and S4. We find these distributions are generally in good agreement with each other suggesting that our model accurately captures the characteristics of LLDPE on short length scales. We then compare our coarse-grain model to the experiments of Orski and coworkers.<sup>4</sup> These experiments are ideal for comparison to our model because the synthetic chemistry used fixes branch spacings and lengths for a given architec-

ture rather than randomly varying these parameters as in most experimental data. Figures 2A and 2B display the radius of gyration and intrinsic viscosity for polymers with a branch spacing of  $S = 8$  carbons and branch lengths of  $L = 0$  (high-density polyethylene), 2, 4, 6, and 10 carbons. Here, we find that all branch lengths exhibit power-law scaling behavior. At constant molar mass as branch length increases, we see that both the radius of gyration and intrinsic viscosity decrease, consistent with the experimental results. Furthermore, our simulations are in good quantitative agreement with experiments. We find that extrapolations from our simulations exhibit 5% average error from experiments.

We also consider the shape factor ( $\rho = R_g/R_h$ ), Fig. 2C. This result has significantly more noise than  $R_g$  and  $[\eta]$  because it is a ratio of two quantities each with its own uncertainty. However, we find a general trend that longer branch lengths show lower shape factors. While we expect randomly branched and comb-like polymers to reside in different scaling regimes, this result is consistent with experimental results<sup>34</sup> that show branched polymers have decreased shape factors compared to linear polymers. The shape factor also compares well with experimental results for linear polyethylene<sup>34</sup> denoted by the dashed line.

To better quantify these results, we extract the scaling exponents and prefactors that characterize Eqs. 1-3. While many works<sup>4,25</sup> fit independent scaling exponents for different architectures, within uncertainty, we see no change in the scaling exponents in our data as shown in Figs. 2A and 2B, suggesting our comb-like polymers belong to the same scaling regime of polymer architecture. Moreover, we note that prior experimental works have made similar assumptions.<sup>2</sup> Thus, we fit our data with an architecture dependent prefactor and a single, universal scaling exponent for each dilute solution property. These fits, shown in Figs. 2A and 2B, quantitatively match our data well. The exponents we obtain are  $\nu_{R_g} = 0.594 \pm 0.003$ ,  $\nu_{[\eta]} = 0.684 \pm 0.005$ , and  $\nu_{R_h} = 0.550 \pm 0.002$  where the error bars represent standard deviations. These results are within the measurement error of experiments,<sup>4</sup> and agree reasonably well with the expected theoretical value for the radius of gyration scaling exponent,  $\nu_{R_g} = 0.588 \pm 0.001$ .<sup>12</sup>

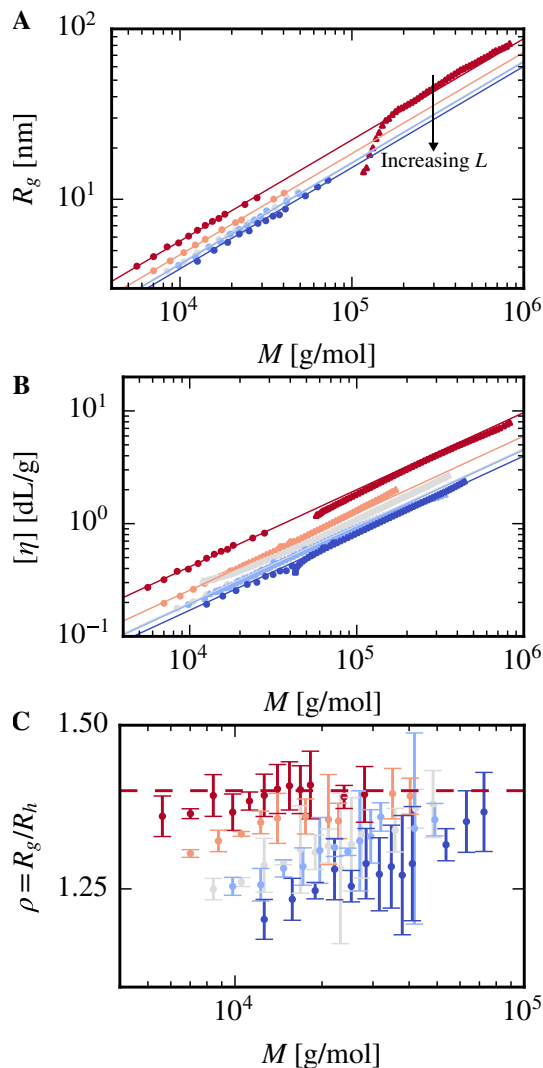


Figure 2: **Comparison of coarse-grain model to experimental data.** Plots show the (A) radius of gyration ( $R_g$ ), (B) intrinsic viscosity ( $[\eta]$ ), and (C) shape factor ( $\rho = R_g/R_h$  where  $R_h$  is the hydrodynamic radius) as a function of molar mass ( $M$ ). Results from molecular dynamics simulations of LLDPE with a branch spacing of  $S = 8$  carbons are displayed as dots. As we go from red to blue, the branch length of the LLDPE increases from  $L = 0$  (high density polyethylene), 2, 4, 6, and 10 carbons. Plots (A) and (B) also show experimental data from Orski and coworkers<sup>4</sup> for the same architectures represented by triangles at high molar mass. Experimental radius of gyration data was excluded from (A) for all but the high density polyethylene sample because uncertainty in the differential refractive index made other architectures unreliable. The constant rescaling factor ( $c$ ) is used to align the intrinsic viscosity computed with ZENO with experiments in (B) as discussed in the Methods section. Solid lines in (A) and (B) are power-law fits to the molecular dynamics data using the same scaling exponents across all architectures. The dashed red line in (C) shows the average  $\rho$  for linear PE.<sup>34</sup> The error bars in (C) are generated by taking the bootstrap standard error of 3 independent simulations.

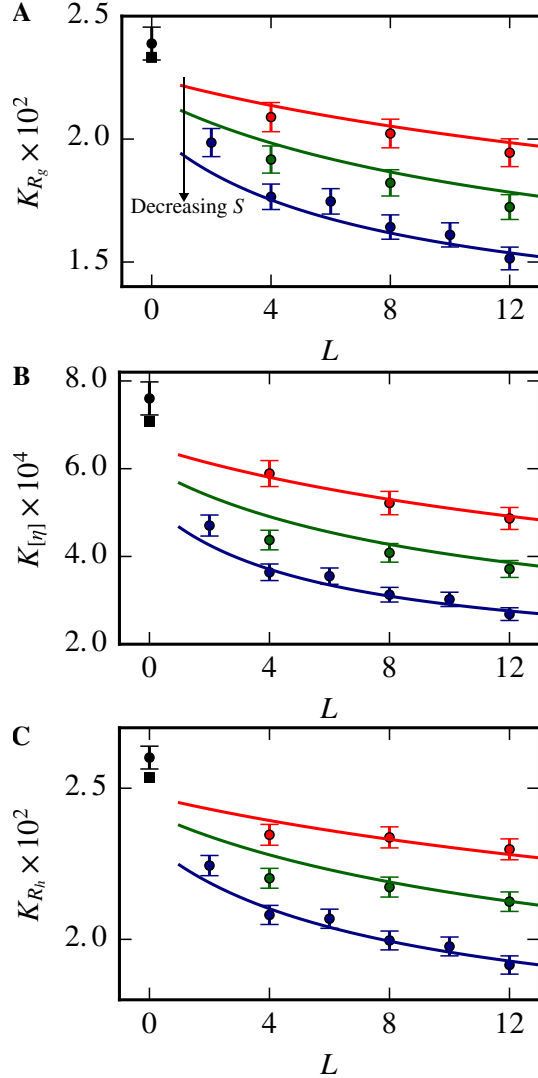


Figure 3: **Coarse-grain model prefactors.** Plots show prefactors of (A) radius of gyration ( $K_{R_g}$ ), (B) intrinsic viscosity ( $K_{[\eta]}$ ), and (C) hydrodynamic radius ( $K_{R_h}$ ) as functions of branch length ( $L$ ) in carbons. The colors blue, green, and red represent branch spacings ( $S$ ) of  $S = 8, 16,$  and  $32$  carbons between branches. Black is the prefactor for polyethylene. Circles represent prefactors from our coarse-grain model. Error bars denote the standard deviations. Lines and squares denote predictions of our comb-like polymer model.

We present the corresponding scaling prefactors in Fig. 3. We see a downward shift of these scaling prefactors for all dilute solution properties as we increase branch length and decrease branch spacing. Some curvature exists at low branch lengths for small branch spacings ( $S = 8$  carbons), while less curvature exists at large branch spacings ( $S = 16$  and  $32$  carbons).

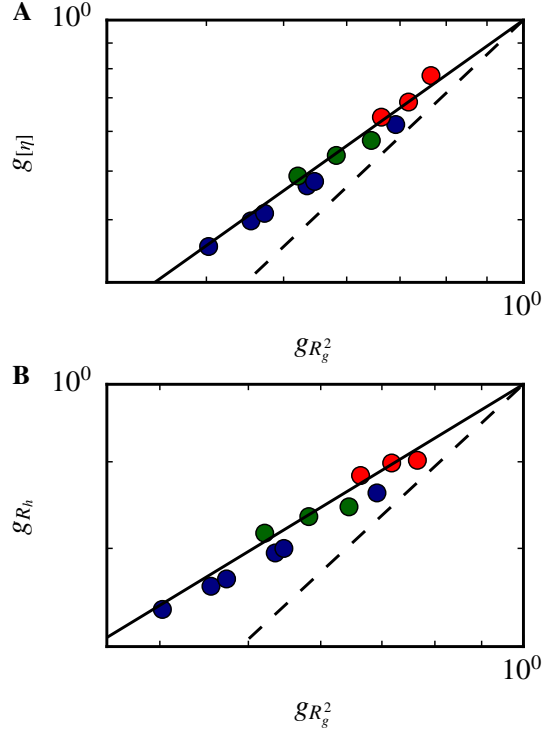


Figure 4: **Contraction factors of coarse-grain model.** Plots show contraction factors of (A) intrinsic viscosity ( $g_{[\eta]}$ ) and (B) the hydrodynamic radius ( $g_{R_h}$ ) against the contraction factor of the radius of gyration ( $g_{R_g^2}$ ). The colors blue, green, and red represent branch spacings ( $S$ ) of  $S = 8, 16,$  and  $32$  carbons between branches. The dashed lines are power laws using theoretically predicted exponents ( $\epsilon_{[\eta]} = 3/2$  and  $\epsilon_{R_h} = 1/2$ , respectively) while the solid lines are power laws found by fitting our theoretical model to the available data ( $\epsilon_{[\eta]} = 1.13 \pm 0.03$  and  $\epsilon_{R_h} = 0.33 \pm 0.02$ , respectively).

Using the scaling prefactors, we compute the contraction factors and examine the relationship between the contraction factor of the radius of gyration and the contraction factors of intrinsic viscosity and the hydrodynamic radius in Fig. 4. The data is nearly linear on a log-log scale, indicating a power-law relationship between the contraction factors as postulated in Eqs. 7 and 8. These power-laws show significant deviation from the power law predicted by the Flory-Fox relationship and the non-draining model that suggest  $\epsilon_{[\eta]} = 3/2$  and  $\epsilon_{R_h} = 1/2$ .<sup>11</sup> Moreover, we see no apparent change in these power-laws as a function of branch spacing or length. We review the implications of this result in further detail in the Discussion section.

## Theoretical model and scaling collapse

To better understand our results, we build a physically inspired model for comb-like macromolecules. While previous work has developed models of the conformational properties of comb-like polymers in good solvent<sup>47–49</sup> based on Flory free energy arguments as compared to experiments recently,<sup>50</sup> we take a geometric approach that is motivated by our coarse-grain model. We begin with the excess mass per unit backbone length that the branches of these polymers add compared to their linear counterparts. Consider a linear polymer with linear branches of length  $L$  units, a branch spacing of  $S$  units, and the same backbone length as a linear polymer with mass  $M_l$ . The mass of this comb-like macromolecule is  $M_C = (1 + L/S)M_l$ . If these branches do not change the chain configuration and only add mass to the macromolecule, we would expect a radius of gyration scaling relation similar to Eq. 1,

$$R_g = K_{R_g}^l (\gamma M)^{\nu_{R_g}} \quad (10)$$

where  $K_{R_g}^l$  is the prefactor of the radius of gyration scaling relationship for the linear polymer, and  $\gamma = 1/(1 + L/S)$  is a mass rescaling factor for the branched polymer. We may interpret  $L/S$  as the excess mass per unit backbone length.

To fully capture the physics of comb-like macromolecules, we must make two additional modifications to this theory to account for changes in the persistence length of the backbone due to the addition of branches. First, excluded volume effects at the branching point cause the backbone of polymer chains to kink. We observe this effect for LLDPE directly in Fig. 1C where the distribution of  $X$ - $A$ - $X$  bond angles (backbone angles *without* branches) is straighter than  $X$ - $B$ - $X$  bond angles (backbone angles *with* branches). Suppose the dihedral angle energies are relatively small compared to our bond length and bond angle energies, as is typical when coarse-graining over a few atoms. In that case, we can expect to account for this effect using a modification of the freely rotating chain model. In this model, the persistence length of a linear polymer is  $l_p^l \propto 1/\ln(\langle \cos(\theta_{XAX}) \rangle)$ .<sup>11</sup> For a comb-like macromolecule with

branch spacing of  $S'$  coarse-grained monomers, or equivalently  $S/4$  carbons, the percentage of monomers along the backbone with branches is  $1/S'$ . Assuming these branches occur at random locations in the chain, we can follow the derivation of the persistence length for a freely rotating chain to obtain

$$l_p^b \propto \frac{1}{\ln(1/S' \langle \cos(\theta_{\text{XBX}}) \rangle) + (1 - 1/S') \langle \cos(\theta_{\text{XAX}}) \rangle} \quad (11)$$

in monomer units. This expression suggests the ratio of LLDPE to high density polyethylene persistence lengths due to kinks

$$\delta_k = \frac{\ln(\langle \cos(\theta_{\text{XAX}}) \rangle)}{\ln(4/S \langle \cos(\theta_{\text{XBX}}) \rangle) + (1 - 4/S) \langle \cos(\theta_{\text{XAX}}) \rangle} \quad (12)$$

where the factor of 4 comes from the number of carbons in coarse-grain monomers along the backbone, as shown in Fig. 1A, and measuring  $S$  in carbons. Using an alternative coarse-graining scheme with a different number of carbons along the backbone would change this factor as well as the bond angles employed, yielding quantitatively similar results.

The second effect that modifies the persistence length is inter-branch repulsion. To understand this effect, we consider how inter-branch repulsion changes the branched to linear polymer persistence length ratio,  $\delta_r \approx 1 + \Delta l$ . Modeling the backbone between the branches as a spring, we see that  $\Delta l$  should be proportional to the force between the branches, which is proportional to the number of interactions between the branches. The number of interactions between branches should be roughly proportional to the area that the branch occupies, similar to number collisions between a gas and a piston at constant pressure. Thus, we should expect  $\Delta l \propto R_g^2(L)$  where  $R_g^2(L)$  is the squared radius of gyration of a branch  $L$  units long. Dimensional analysis suggests that  $\Delta l \propto R_g^2(L)/R_g^2(S)$  where  $S$  is the spacing between branches. Assuming that both the branch length and spacing are long enough to exhibit scaling behavior and that the branches and backbone are in a good solvent regime, we expect  $\Delta l \propto (L/S)^{6/5}$  where we use the Flory theory exponent,  $\nu_{R_g} = 3/5$ , for simplicity.

Thus, we expect

$$\delta_r = 1 + C \left( \frac{L}{S} \right)^{6/5} \quad (13)$$

where  $C$  is a constant that measures the repulsive force between branches at a given concentration and temperature.

Given these two contributions, we surmise that the total ratio of comb-like to linear polymer persistence lengths is  $l_p^b/l_p^l = \delta_k \delta_r$ . Flory theory<sup>11</sup> suggests that this modification to persistence length should modify Eq. 10 such that

$$R_g = \lambda_{R_g} K_{R_g}^l (\gamma M)^{\nu_{R_g}} \quad (14)$$

where  $\lambda_{R_g} = (\delta_k \delta_r)^{2/5}$ .

Having determined a general theory for  $R_g$ , we employ relationships between our contraction factors (Eqs. 7 and 8) as well as the observation that  $\epsilon_{[\eta]}$  and  $\epsilon_{R_h}$  are constant for lightly branched polymers, as shown in Fig. 4, to derive

$$[\eta] = \lambda_{[\eta]} K_{[\eta]}^l (\gamma M)^{\nu_{[\eta]}} \quad (15)$$

$$R_h = \lambda_{R_h} K_{R_h}^l (\gamma M)^{\nu_{R_h}} \quad (16)$$

where  $\lambda_{[\eta]} = \gamma^{-\nu_{[\eta]}} (\lambda_{R_g} \gamma^{\nu_{R_g}})^{2\epsilon_{[\eta]}}$  and  $\lambda_{R_h} = \gamma^{-\nu_{R_h}} (\lambda_{R_g} \gamma^{\nu_{R_g}})^{2\epsilon_{R_h}}$ .

We fit our LLDPE data to this model, fixing the scaling exponents we found previously and the average angles ( $\langle \cos(\theta) \rangle_{XAX} = 0.7465$  and  $\langle \cos(\theta) \rangle_{XBX} = 0.5842$ ) to the molecular dynamics results. We find  $C = 0.56 \pm 0.03$ ,  $K_{R_g}^l / 10^{-2} = 2.33 \pm 0.01$ ,  $K_{[\eta]}^l / 10^{-4} = 7.08 \pm 0.05$ ,  $K_{R_h}^l / 10^{-2} = 2.53 \pm 0.02$ ,  $\epsilon_{[\eta]} = 1.13 \pm 0.03$ , and  $\epsilon_{R_h} = 0.33 \pm 0.02$ . The error bars represent standard deviations. In principle, we can fix all values except  $C$  by directly fitting the data in Figs. 3 and 4, but this approach leads to the error in the scaling prefactors of high density polyethylene propagating throughout the calculation, whereas globally fitting reduces this uncertainty. We now plot the scaling collapses for our dilute solution properties for a set

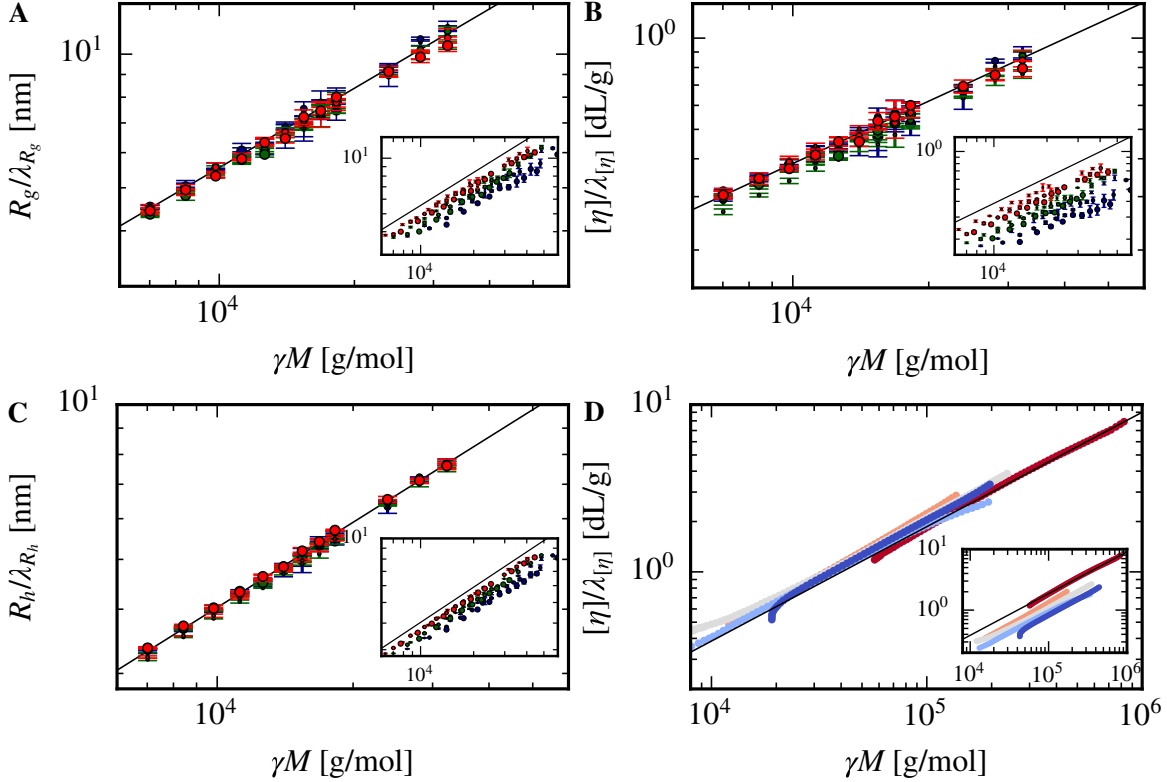


Figure 5: **Scaling collapse.** Plots show scaling collapse of (A) the radius of gyration, (B) intrinsic viscosity, and (C) the hydrodynamic radius for simulated data using the theory (Eqs. 14-16). We use the color scheme from Fig. 3 to denote different branch spacing. Point sizes (small, medium, and large) denote branch lengths of  $L = 4, 8,$  and  $12,$  respectively. Lines are high density polyethylene scaling relationships. (D) Plot shows the scaling collapse of experimental data of Orski and coworkers<sup>4</sup> for branch spacing  $S = 8$  carbons. We use the color scheme from Fig. 2 to denote branch lengths. In each plot, the inset shows data prior to scaling transformation. Error bars are generated by taking the bootstrap standard error of 3 independent simulations.

of selected molecular dynamics data in Figs. 5A, 5B, and 5C. Additionally, we plot the scaling collapse of the experimental data of Orski and coworkers<sup>4</sup> in Fig. 5D. We find that in all cases, the scaling collapse is excellent. As a further check of these results, we plot the predictions our model makes against our molecular dynamics data for our prefactors and contraction factors in Figs. 3 and 4. The comparison is good in both cases. In the case of Fig. 3, we find that the theory is mostly within the error bars of the prefactor fits. For Fig. 4, we find the fits have  $R^2 \geq 0.97$  in both cases.

## Discussion

This work develops an implicit solvent, coarse-grain force field for LLDPE in 1,2,4-trichlorobenzene. At short length scales (low molar mass), this force field replicates all-atom bond length, angle, and dihedral monomer distributions. At long length scales (high molar mass), it extrapolates to the experimental results of Orski and coworkers.<sup>4</sup> This model allows for the scaling analysis of the radius of gyration, intrinsic viscosity, and hydrodynamic radius of LLDPE in a good solvent. In particular, we find that the contraction exponents, as defined in Eqs. 7 and 8, do not depend on branch length or spacing but also do not match theoretical predictions ( $\epsilon_{[\eta]} = 1.13 \pm 0.03 \neq 3/2$  and  $\epsilon_{R_h} = 0.33 \pm 0.02 \neq 1/2$ ). Finally, we consider a general theory to explain the scaling behavior of lightly branched comb-like macromolecules. This theory rescales the mass and the persistence length of these polymers to obtain a radius of gyration scaling relationship. Using our empirically constant contraction exponents, we obtain scaling relationships for intrinsic viscosity and the hydrodynamic radius.

We begin by discussing the practical ramifications of our work. First, our coarse-grain model and subsequent theory provide high-quality benchmarks that may be compared to industrial LLDPE feedstocks that lack the precise architecture of the model materials studied here. We can leverage such benchmarks as a tool to determine the architecture in these feedstocks more precisely through dilute solution characterization. Then, we can correlate this structure with bulk LLDPE properties. Because branch lengths and spacings are uncertain in industrial LLDPE, these comparisons cannot be one-to-one. Assuming the probability distributions of branch lengths and spacings do not change along the polymer backbone, our theory suggests that we can combine these distributions with  $\delta_k$  and  $\delta_r$  (Eqs. 12 and 13) to obtain a modified persistence length ratio. Obtaining this ratio immediately leads to expressions for the radius of gyration, intrinsic viscosity, and hydrodynamic radius given constant contraction exponents. Similarly, we may be able understand the structure of polymers generated using chain walking catalysis at low walking rates<sup>51</sup> given reasonable modifications to the form of the mass rescaling factor ( $\gamma$ ) and repulsion factor ( $\delta_r$ ) that account for the

non-linear nature of the branches. Further development and testing is needed to verify these relationships.

Next, we consider commonly studied dimensionless ratios of dilute solution properties. The values of these ratios are often compared to theoretical values for hard spheres and rigid rods to better understand the shape of the polymer. Our theory makes explicit predictions about these ratios for comb-like macromolecules that clarify how they should depend on chain architecture. First, it suggests the shape factor<sup>25,34</sup> takes the form,

$$\rho = R_g/R_h \propto (\gamma^{\nu_{R_g}} \lambda_{R_g})^{(1-2\epsilon_{R_h})} \quad (17)$$

where we have excluded the prefactors and the weak mass dependence ( $M^{\nu_{R_g}-\nu_{R_h}} = M^{0.044}$ ) for clarity. While the mass rescaling function ( $\gamma$ ) decreases with the addition of branches (decreasing  $S$ ) or as branches grow (increasing  $L$ ), a competition between forces causes the radius of gyration rescaling factor ( $\lambda_{R_g}$ ) to be non-monotonic. For lightly branched polymers (small  $L$  and large  $S$ ), this rescaling factor decreases as we add branches indicating a more sphere-like configuration due to the kinks formed by attaching branches to the backbone. Decreasing branch spacing further causes this radius of gyration rescaling factor to increase as chains begin to repulse each other. The non-monotonic nature of the radius of gyration rescaling factor ( $\lambda_{R_g}$ ) causes the shape factor ( $\rho$ ) to decrease slower at large  $L$ . We show our theory's prediction for this quantity in the Supporting Information, Fig. S7.

Another dimensionless ratio, the topology factor ( $\kappa = R_{[\eta]}/R_g$ ) provides similar qualitative information about the shape of the polymer.<sup>25,34,52</sup> Here,  $R_{[\eta]} = \left(\frac{3[\eta]M}{10\pi N_A}\right)^{1/3}$ , is the viscometric radius. Our model yields

$$\kappa \propto (\gamma^{\nu_{R_g}} \lambda_{R_g})^{(2\epsilon_{[\eta]}/3-1)} \quad (18)$$

where we have again excluded prefactors and weak mass dependence ( $M^{(\nu_{[\eta]}+1)/3-\nu_{R_g}} = M^{-0.032}$ ). Comparing the shape and topology factors, we find that these ratios are related

by a power law with an exponent of approximately  $-1$ . As such, the above arguments about the shape factor also hold for the topology factor in reverse. This relationship also clarifies the negative correlation between these factors as seen in experiments.<sup>34</sup>

We now discuss the more theoretical ramifications of our work. We first consider our constant contraction exponents. These contraction exponents deviate significantly from the Flory-Fox relation ( $\epsilon_{[\eta]} = 3/2$ ) and non-draining model ( $\epsilon_{R_h} = 1/2$ ). Moreover, they do not seem to systematically vary as we change branch length or spacing in contrast to the suggestion by Berry.<sup>19</sup> As first postulated in Lee and Chang<sup>3</sup> for polystyrene comb-like polymers, the intrinsic viscosity contraction exponents are constant and approximately unity ( $\epsilon_{[\eta]} \approx 1$ ) in a good solvent. Our observation of this phenomenon lends additional credibility to this argument as we have a complete control over the structure of our polymers *in silico* and find  $\epsilon_{[\eta]} = 1.13 \pm 0.03$ . Furthermore, this observation adds to the growing evidence of the inadequacy of the Flory-Fox relationship when predicting prefactors.<sup>53,54</sup>

Indeed, our observation of constant scaling and contraction exponents indicate that comb-like polymers reside in a single scaling regime. The architectural limits on this regime are unclear. Certainly, star polymers have different exponents<sup>20,21</sup> and may be thought of as comb-like polymers where the backbone length ( $N$ ) is much less than the branch length ( $N \ll L$ ). We can further ask whether bottlebrush polymers (large  $L$  and small  $S$ ) reside in a different regime. Vargas-Lara *et al.*<sup>16</sup> find that worm-like chains have different scaling exponents than more flexible polymers. This observation suggests a separate regime in the bottlebrush limit in which inter-branch repulsion dramatically increases the persistence length. Gay and Raphaël<sup>55</sup> use simple Flory free energy methods to postulate that a transition between comb-like and bottlebrush polymers occurs when  $L \gg S^3$  and between comb-like and star polymers occurs when  $L \gg S^3 \gg N$ . We check these limits by comparing our theory to experimental bottlebrush polymer data in the Supporting Information, Fig. S8. Despite using several approximations in our comparison, we find that our model performs surprisingly well without modifying the exponents.

While the architectural limits of our constant scaling and contraction exponents remain unclear, we understand that the approximate expression for the change in persistence length ( $\delta$ ) breaks down under certain circumstances. First, we would expect changes in  $\delta_k$ , Eq. 12, when branch spacing becomes smaller than the coarse-grain monomer size, *i.e.*  $S < 4$  carbons. In this case, we may approximate  $\delta_k$  as the value of  $\delta_k$  for  $S = 4$  if we assume the backbone is rod-like below this length scale. Second, we apply scaling theory to the branch spacings and lengths in a good solvent to obtain an expression for  $\delta_r$ , Eq. 13. However, scaling theory is not valid for small branch spacings or lengths. Indeed, the most significant deviations from our theory occur when  $L = 2$  or  $4$  in Fig. 3. This observation suggests that accurately dealing with small branch spacings and lengths in which the geometry of the carbon-carbon bonds plays a significant role would require a more detailed theory.

We next examine how our theory compares to that of other works. In particular, Vargas-Lara *et al.*<sup>16</sup> have recently suggested a general interrelation between the dilute solution properties that we have studied,

$$[\eta] = \frac{0.79N_A}{M} 4\pi R_h^{1/\nu_{R_g}} R_g^{(3\nu_{R_g}-1)/\nu_{R_g}} \quad (19)$$

where  $N_A$  is Avogadro's number. This theory indicates relationships between our scaling and contraction exponents. In particular, we find  $\nu_{[\eta]} = (3\nu_{R_g} - 1) + (\nu_{R_h}/\nu_{R_g} - 1) = 0.707 \pm 0.005$  and  $\epsilon_{[\eta]} = 3/2 + (\epsilon_{R_h} - 1/2)/\nu_{R_g} = 1.21 \pm 0.03$ . These values are similar to our scaling ( $\nu_{[\eta]} = 0.684 \pm 0.005$ ) and contraction ( $\epsilon_{[\eta]} = 1.13 \pm 0.03$ ) exponents and will produce quantitatively similar results for intrinsic viscosity. However, close examination yields that the scaling exponents are more than 3 standard deviations away from each other, suggesting a possible more detailed theory relating these terms. Nevertheless, this theory is at least approximately true in our case and superior to the Flory-Fox prediction.

Last, we turn to future uses of our coarse-grain force-field. Because we have ensured that our model captures short and long-range behavior of the polymer in the solvent, this model

for LLDPE in 1,2,4-trichlorobenzene, a standard good solvent for polyolefins,<sup>2,4,34</sup> should extrapolate to structures outside of the comb-like structures we have examined here. We can efficiently manufacture structures such as diblock, ladder, ring, hyperbranched polymers, and industrially relevant LLDPE *in silico* and directly compare to experiments using our existing model. To study bottlebrush polymers, we would only need to run a limited number of additional all-atom molecular dynamics simulations to obtain the bonded interactions.

## Conclusions

We have designed a coarse-grain, implicit solvent model of LLDPE in 1,2,4-trichlorobenzene, a common polymer-good solvent pair. This model reproduces all-atom bond distributions and experimental results, suggesting it is valid at all length scales. We then extend a library of structure-dilute solution properties of LLDPE with precise branch lengths and spacings in a good solvent. This data demonstrates that the contraction exponents for intrinsic viscosity and the hydrodynamic radius ( $\epsilon_{[\eta]}$  and  $\epsilon_{R_h}$ ) remain constant as branch length and spacing is varied. These results motivate our theory for the scaling of dilute solution properties of comb-like macromolecules in a good solvent. While the architectural limits of this theory remain unclear, we find that it represents all data in the library we have developed reasonably well. This theory provides insight into how to infer structure from dilute solution properties allowing for the tuning of multiple properties or the extrapolation of properties from previously studied structure-property relationships for comb-like polymers.

## Acknowledgement

This work was funded by the NRC Research Associateship Program. We would like to thank Dr. Chase B. Thompson and Dr. Jack F. Douglas for many helpful conversations. We thank our collaborators Dr. Kathryn L. Beers, Dr. Marc A. Hillmyer, Dr. Luke A. Kassekert, (Department of Chemistry, University of Minnesota) and Dr. Wesley S. Farrell (Chemistry

Department, US Naval Academy) for the synthesis of model LLDPE polymers used in Ref. 4.

## Supporting Information Available

Supporting Information: Additional information on all-atom simulations, coarse-grain bonded interactions, coarse-grain nonbonded interactions, shape factor predictions as a function of branch length and spacing, and a comparison of experimental bottlebrush contraction factors against theoretical predictions.

Data: Study data and force field parameters are available at <https://doi.org/10.18434/mds2-2494>.

## References

- (1) Flory, P. J.; Volkenstein, M. Statistical mechanics of chain molecules. *Biopolymers* **1969**, *8*, 699–700, \_eprint: <https://onlinelibrary.wiley.com/doi/pdf/10.1002/bip.1969.360080514>.
- (2) Sun, T.; Brant, P.; Chance, R. R.; Graessley, W. W. Effect of Short Chain Branching on the Coil Dimensions of Polyolefins in Dilute Solution. *Macromolecules* **2001**, *34*, 6812–6820, Publisher: American Chemical Society.
- (3) Lee, S.; Chang, T. Branching Analysis of Comb-Shaped Polystyrene with Long Chain Branches. *Macromolecular Chemistry and Physics* **2017**, *218*, 1700087, \_eprint: <https://onlinelibrary.wiley.com/doi/pdf/10.1002/macp.201700087>.
- (4) Orski, S. V.; Kassekert, L. A.; Farrell, W. S.; Kenlaw, G. A.; Hillmyer, M. A.; Beers, K. L. Design and Characterization of Model Linear Low-Density Polyethylenes (LLDPEs) by Multidetector Size Exclusion Chromatography. *Macromolecules* **2020**, *53*, 2344–2353, Publisher: American Chemical Society.

- (5) Liberman-Martin, A. L.; Chu, C. K.; Grubbs, R. H. Application of Bottlebrush Block Copolymers as Photonic Crystals. *Macromolecular Rapid Communications* **2017**, *38*, 1700058, \_eprint: <https://onlinelibrary.wiley.com/doi/pdf/10.1002/marc.201700058>.
- (6) Deng, H.; Dai, F.; Ma, G.; Zhang, X. Theranostic Gold Nanomicelles made from Biocompatible Comb-like Polymers for Thermochemotherapy and Multifunctional Imaging with Rapid Clearance. *Advanced Materials* **2015**, *27*, 3645–3653, \_eprint: <https://onlinelibrary.wiley.com/doi/pdf/10.1002/adma.201501420>.
- (7) Gamarra, A.; Muñoz-Guerra, S.; Martínez de Ilarduya, A.; Thérien-Aubin, H.; Landfester, K. Comblike Ionic Complexes of Hyaluronic Acid and Alkanoylcholine Surfactants as a Platform for Drug Delivery Systems. *Biomacromolecules* **2018**, *19*, 3669–3681, Publisher: American Chemical Society.
- (8) Rabnawaz, M.; Wyman, I.; Auras, R.; Cheng, S. A roadmap towards green packaging: the current status and future outlook for polyesters in the packaging industry. *Green Chemistry* **2017**, *19*, 4737–4753, Publisher: Royal Society of Chemistry.
- (9) Wypych, G. *Handbook of material weathering*; 2003.
- (10) Robertson, G. L. *Food Packaging: Principles and Practice, Second Edition*, 2nd ed.; CRC Press: Boca Raton, 2005.
- (11) Rubinstein, M.; Colby, R. H. *Polymer physics*; Oxford University Press: New York, 2003; Vol. 23.
- (12) Guida, R.; Zinn-Justin, J. Critical exponents of the N-vector model. *Journal of Physics A: Mathematical and General* **1998**, *31*, 8103–8121, Publisher: IOP Publishing.
- (13) Douglas, J. F.; Freed, K. F. Competition between Hydrodynamic Screening (“Draining”) and Excluded Volume Interactions in an Isolated Polymer Chain. *Macromolecules* **1994**, *27*, 6088–6099.

- (14) Mansfield, M. L.; Tsortos, A.; Douglas, J. F. Persistent draining crossover in DNA and other semi-flexible polymers: Evidence from hydrodynamic models and extensive measurements on DNA solutions. *The Journal of Chemical Physics* **2015**, *143*, 124903, Publisher: American Institute of Physics.
- (15) Lu, Y.; An, L.; Wang, Z.-G. Intrinsic Viscosity of Polymers: General Theory Based on a Partially Permeable Sphere Model. *Macromolecules* **2013**, *46*, 5731–5740, Publisher: American Chemical Society.
- (16) Vargas-Lara, F.; Mansfield, M. L.; Douglas, J. F. Universal interrelation between measures of particle and polymer size. *J. Chem. Phys.* **2017**, *9*.
- (17) Hadjichristidis, N.; Lindner, J. S.; Mays, J. W.; Wilson, W. W. Sub- $\theta$  hydrodynamic behavior of poly( $\alpha$ -methylstyrene) in cyclohexane. *Macromolecules* **1991**, *24*, 6725–6729, Publisher: American Chemical Society.
- (18) Zimm, B. H.; Kilb, R. W. Dynamics of branched polymer molecules in dilute solution. *Journal of Polymer Science* **1959**, *37*, 19–42, eprint: <https://onlinelibrary.wiley.com/doi/pdf/10.1002/pol.1959.1203713102>.
- (19) Berry, G. C. Thermodynamic and conformational properties of polystyrene. III. Dilute solution studies on branched polymers. *Journal of Polymer Science Part A-2: Polymer Physics* **1971**, *9*, 687–715, eprint: <https://onlinelibrary.wiley.com/doi/pdf/10.1002/pol.1971.160090410>.
- (20) Kurata, M.; Abe, M.; Iwama, M.; Matsushima, M. Randomly Branched Polymers. I. Hydrodynamic Properties. *Polymer Journal* **1972**, *3*, 729–738, Bandiera\_abtest: a Cg\_type: Nature Research Journals Number: 6 Primary\_atype: Research Publisher: Nature Publishing Group.
- (21) Roovers, J.; Toporowski, P. M.; Douglas, J. Thermodynamic Properties of Dilute and Semidilute Solutions of Regular Star Polymers. *Macromolecules* **1995**, *28*, 7064–7070.

- (22) Farmer, B. S.; Terao, K.; Mays, J. W. Characterization of Model Branched Polymers by Multi-Detector SEC in Good and Theta Solvents. *International Journal of Polymer Analysis and Characterization* **2006**, *11*, 3–19, Publisher: Taylor & Francis .eprint: <https://doi.org/10.1080/10236660500484213>.
- (23) Radke, W.; Müller, A. H. E. Synthesis and Characterization of Comb-Shaped Polymers by SEC with On-Line Light Scattering and Viscometry Detection. *Macromolecules* **2005**, *38*, 3949–3960, Publisher: American Chemical Society.
- (24) Hadjichristidis, N. et al. Well-Defined, Model Long Chain Branched Polyethylene. 1. Synthesis and Characterization. *Macromolecules* **2000**, *33*, 2424–2436, Publisher: American Chemical Society.
- (25) López-Barrón, C. R.; Vargas-Lara, F.; Kang, S. Single-Chain Conformation of Poly( $\alpha$ -olefins) in Dilute Solutions at the Crossover between Linear and Bottlebrush Architectures. *Macromolecules* **2021**, *54*, 6854–6866, Publisher: American Chemical Society.
- (26) Shinoda, W.; DeVane, R.; Klein, M. L. Multi-property fitting and parameterization of a coarse grained model for aqueous surfactants. *Molecular Simulation* **2007**, *33*, 27–36, Publisher: Taylor & Francis .eprint: <https://doi.org/10.1080/08927020601054050>.
- (27) Maerzke, K. A.; Siepmann, J. I. Transferable Potentials for Phase Equilibria-Coarse-Grain Description for Linear Alkanes. *The Journal of Physical Chemistry B* **2011**, *115*, 3452–3465, Publisher: American Chemical Society.
- (28) Salerno, K. M.; Agrawal, A.; Perahia, D.; Grest, G. S. Resolving Dynamic Properties of Polymers through Coarse-Grained Computational Studies. *Physical Review Letters* **2016**, *116*, 058302, Publisher: American Physical Society.
- (29) Salerno, K. M.; Agrawal, A.; Peters, B. L.; Perahia, D.; Grest, G. S. Dynamics in

- entangled polyethylene melts. *The European Physical Journal Special Topics* **2016**, *225*, 1707–1722.
- (30) Panizon, E.; Bochicchio, D.; Monticelli, L.; Rossi, G. MARTINI Coarse-Grained Models of Polyethylene and Polypropylene. *The Journal of Physical Chemistry B* **2015**, *119*, 8209–8216, Publisher: American Chemical Society.
- (31) Marrink, S. J.; Risselada, H. J.; Yefimov, S.; Tieleman, D. P.; de Vries, A. H. The MARTINI Force Field: Coarse Grained Model for Biomolecular Simulations. *The Journal of Physical Chemistry B* **2007**, *111*, 7812–7824, Publisher: American Chemical Society.
- (32) Zhang, W.; Vargas-Lara, F.; Orski, S. V.; Beers, K. L.; Douglas, J. F. Modeling short-chain branched polyethylenes in dilute solution under variable solvent quality conditions: Basic configurational properties. *Polymer* **2021**, *217*, 123429.
- (33) Martin, M. G.; Siepmann, J. I. Transferable Potentials for Phase Equilibria. 1. United-Atom Description of n-Alkanes. *The Journal of Physical Chemistry B* **1998**, *102*, 2569–2577, Publisher: American Chemical Society.
- (34) Plüschke, L.; Mundil, R.; Sokolohorskyj, A.; Merna, J.; Sommer, J.-U.; Lederer, A. High Temperature Quadruple-Detector Size Exclusion Chromatography for Topological Characterization of Polyethylene. *Analytical Chemistry* **2018**, *90*, 6178–6186, Publisher: American Chemical Society.
- (35) Hayano, S.; Nakama, Y. Iso- and Syndio-Selective ROMP of Norbornene and Tetracyclododecene: Effects of Tacticity Control on the Hydrogenated Ring-Opened Poly(cycloolefin)s. *Macromolecules* **2014**, *47*, 7797–7811, Publisher: American Chemical Society.
- (36) Jorgensen, W. L.; Maxwell, D. S.; Tirado-Rives, J. Development and Testing of the OPLS All-Atom Force Field on Conformational Energetics and Properties of Organic

- Liquids. *Journal of the American Chemical Society* **1996**, *118*, 11225–11236, Publisher: American Chemical Society.
- (37) Price, M. L. P.; Ostrovsky, D.; Jorgensen, W. L. Gas-phase and liquid-state properties of esters, nitriles, and nitro compounds with the OPLS-AA force field. *Journal of Computational Chemistry* **2001**, *22*, 1340–1352, eprint: <https://onlinelibrary.wiley.com/doi/pdf/10.1002/jcc.1092>.
- (38) Weeks, J. D.; Chandler, D.; Andersen, H. C. Role of Repulsive Forces in Determining the Equilibrium Structure of Simple Liquids. *The Journal of Chemical Physics* **1971**, *54*, 5237–5247, Publisher: American Institute of Physics.
- (39) Hudson, G. H.; McCoubrey, J. C. Intermolecular forces between unlike molecules. A more complete form of the combining rules. *Transactions of the Faraday Society* **1960**, *56*, 761–766, Publisher: The Royal Society of Chemistry.
- (40) Plimpton, S. Fast Parallel Algorithms for Short-Range Molecular Dynamics. *Journal of Computational Physics* **1995**, *117*, 1–19.
- (41) Douglas, J. F.; Garboczi, E. J. *Advances in Chemical Physics*; John Wiley & Sons, Ltd, 1995; pp 85–153.
- (42) Mansfield, M. L.; Douglas, J. F. Improved path integration method for estimating the intrinsic viscosity of arbitrarily shaped particles. *Physical Review E* **2008**, *78*, 046712.
- (43) Juba, D.; Keyrouz, W.; Mascagni, M.; Brady, M. Acceleration and Parallelization of ZENO/Walk-on-Spheres. *Procedia Computer Science* **2016**, *80*, 269–278.
- (44) Juba, D.; Audus, D. J.; Mascagni, M.; Douglas, J. F.; Keyrouz, W. ZENO: Software for calculating hydrodynamic, electrical, and shape properties of polymer and particle suspensions. *Journal of Research of the National Institute of Standards and Technology* **2017**, *122*, 20.

- (45) Kirkpatrick, S.; Gelatt, C. D.; Vecchi, M. P. Optimization by Simulated Annealing. *Science* **1983**, *220*, 671–680, Publisher: American Association for the Advancement of Science Section: Articles.
- (46) Shirts, M. R.; Chodera, J. D. Statistically optimal analysis of samples from multiple equilibrium states. *The Journal of Chemical Physics* **2008**, *129*, 124105.
- (47) Rouault, Y.; Borisov, O. V. Comb-Branched Polymers: Monte Carlo Simulation and Scaling. *Macromolecules* **1996**, *29*, 2605–2611, Publisher: American Chemical Society.
- (48) Morozova, S.; Lodge, T. P. Conformation of Methylcellulose as a Function of Poly(ethylene glycol) Graft Density. *ACS Macro Letters* **2017**, *6*, 1274–1279, Publisher: American Chemical Society.
- (49) Fredrickson, G. H. Surfactant-induced lyotropic behavior of flexible polymer solutions. *Macromolecules* **1993**, *26*, 2825–2831, Publisher: American Chemical Society.
- (50) Pan, X.; Ding, M.; Li, L. Experimental Validation on Average Conformation of a Comb-like Polystyrene Library in Dilute Solutions: Universal Scaling Laws and Abnormal SEC Elution Behavior. *Macromolecules* **2021**, *54*, 11019–11031, Publisher: American Chemical Society.
- (51) Dockhorn, R.; Plüschke, L.; Geisler, M.; Zessin, J.; Lindner, P.; Mundil, R.; Merna, J.; Sommer, J.-U.; Lederer, A. Polyolefins Formed by Chain Walking Catalysis—A Matter of Branching Density Only? *Journal of the American Chemical Society* **2019**, *141*, 15586–15596, Publisher: American Chemical Society.
- (52) Ostlund, S. G.; Striegel, A. M. Ultrasonic degradation of poly( $\gamma$ -benzyl-L-glutamate), an archetypal highly extended polymer. *Polymer Degradation and Stability* **2008**, *93*, 1510–1514.

- (53) Mansfield, M. L.; Douglas, J. F. Transport Properties of Wormlike Chains with Applications to Double Helical DNA and Carbon Nanotubes. *Macromolecules* **2008**, *41*, 5412–5421, Publisher: American Chemical Society.
- (54) Lederer, A.; Burchard, W.; Khalyavina, A.; Lindner, P.; Schweins, R. Is the Universal Law Valid for Branched Polymers? *Angewandte Chemie International Edition* **2013**, *52*, 4659–4663, eprint: <https://onlinelibrary.wiley.com/doi/pdf/10.1002/anie.201209228>.
- (55) Gay, C.; Raphaël, E. Comb-like polymers inside nanoscale pores. *Advances in Colloid and Interface Science* **2001**, *94*, 229–236.

## Graphical TOC Entry

